

**Electronic Supplementary Information (ESI)**

**Fe–N/C catalysts with tunable mesoporous structure and carbon layer number reveal the role of interlayer O<sub>2</sub> activation**

**Jinwoo Woo,<sup>a</sup> June Sung Lim,<sup>a</sup> Taejung Lim,<sup>b</sup> Du San Baek,<sup>b</sup> Jae Hyung Kim,<sup>c</sup> Jong Hoon Lee,<sup>d</sup> Hu Young Jeong,<sup>e</sup> Chang Hyuck Choi,<sup>f</sup> and Sang Hoon Joo<sup>\*b</sup>**

<sup>a</sup> *School of Energy and Chemical Engineering, Ulsan National Institute of Science and Technology (UNIST), Ulsan 44919, Republic of Korea.*

<sup>b</sup> *Department of Chemistry, UNIST, Ulsan 44919, Republic of Korea. E-mail:  
shjoo@unist.ac.kr*

<sup>c</sup> *Clean Fuel Research Laboratory, Korea Institute of Energy Research, Daejeon 34129, Republic of Korea.*

<sup>d</sup> *UNIST Central Research Facilities, UNIST, Ulsan 44919, Republic of Korea.*

<sup>e</sup> *Graduate School of Semiconductor Materials and Devices Engineering, UNIST, Ulsan 44919, Republic of Korea.*

<sup>f</sup> *Department of Chemistry, Pohang University of Science and Technology (POSTECH), Pohang 37673, Republic of Korea.*

## Table of Contents

<b>1. Supplementary Figures and Tables</b>	<b>S3</b>
<b>Fig. S1</b> SEM images of SBA-15 template and Meso-Fe–N/C_X.	<b>S3</b>
<b>Fig. S2</b> XRD patterns of Meso-Fe–N/C_X.	<b>S4</b>
<b>Fig. S3</b> N <sub>2</sub> adsorption-desorption isotherms and the pore size distribution curves of Meso-Fe–N/C_X.	<b>S5</b>
<b>Table S1.</b> Textural properties of Meso-Fe–N/C_X.	<b>S6</b>
<b>Fig. S4</b> EXAFS fitting curves of Meso-Fe–N/C_1.0 and Meso-Fe–N/C_2.0.	<b>S7</b>
<b>Table S2.</b> EXAFS curve fitting results.	<b>S8</b>
<b>Fig. S5</b> Deconvoluted N 1s and C 1s and O 1s XPS spectra of Meso-Fe–N/C_X.	<b>S9</b>
<b>Table S3.</b> Relative peak areas for the deconvoluted N 1s XPS spectra of Meso-Fe–N/C_X.	<b>S10</b>
<b>Table S4.</b> Elemental analysis results of Meso-Fe–N/C_X.	<b>S11</b>
<b>Fig. S6</b> CO pulse cryo-adsorption profiles of Meso-Fe–N/C_X.	<b>S12</b>
<b>Fig. S7</b> ORR polarization curves and Tafel slopes of Meso-Fe–N/C_X.	<b>S13</b>
<b>Table S5.</b> Site density and ORR activity parameters of Meso-Fe–N/C_X in 0.1 M KOH.	<b>S14</b>
<b>Table S6.</b> Benchmarking the TOF of Meso-Fe–N/C_2.0 with those of reported Fe–N/C catalysts in alkaline media.	<b>S15</b>
<b>Table S7.</b> Site density and ORR activity parameters of Meso-Fe–N/C_X in 0.1 M HClO <sub>4</sub> .	<b>S16</b>
<b>Table S8.</b> Benchmarking the TOF of Meso-Fe–N/C_2.0 with those of reported Fe–N/C catalysts in acidic media.	<b>S17</b>
<b>Fig. S8</b> ORR long-term durability of Meso-Fe–N/C_1.0, Meso-Fe–N/C_2.0, and Pt/C catalysts.	<b>S18</b>
<b>Fig. S9</b> O <sub>2</sub> TPD profiles of Meso-Fe–N/C_X.	<b>S19</b>
<b>Fig. S10</b> N <sub>2</sub> adsorption-desorption isotherms, ORR polarization curves, and activity parameters of Meso-Fe–N/C_X and Meso-Fe–N_C_Fe.	<b>S20</b>
<b>2. References</b>	<b>S21</b>

## 1. Supplementary Figures and Tables

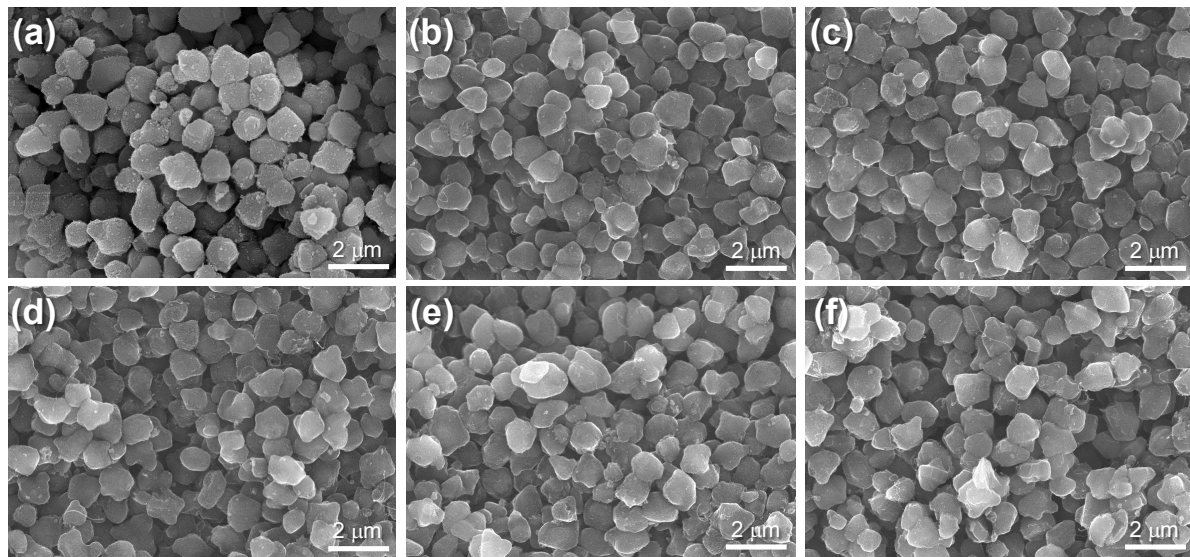


**Fig. S1** SEM images of (a) SBA-15 silica template, (b) Meso-Fe–N/C\_1.0, (c) Meso-Fe–N/C\_1.25, (d) Meso-Fe–N/C\_1.5, (e) Meso-Fe–N/C\_1.75, and (f) Meso-Fe–N/C\_2.0.

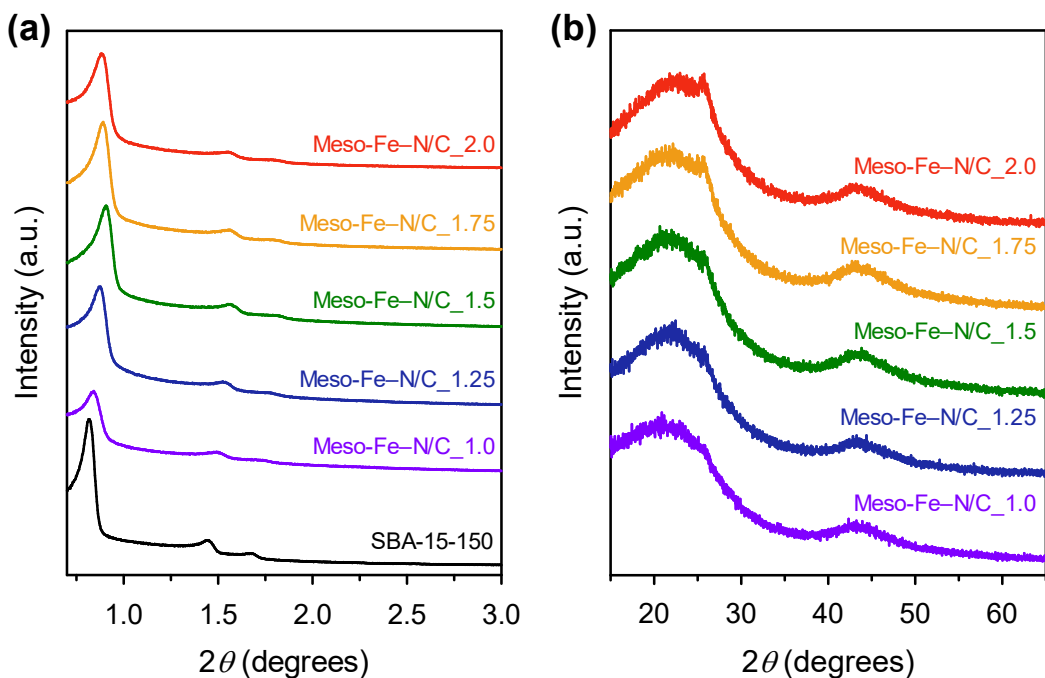


**Fig. S2** (a) Small-angle and (b) wide-angle XRD patterns of the Meso-Fe–N/C<sub>X</sub> catalysts.

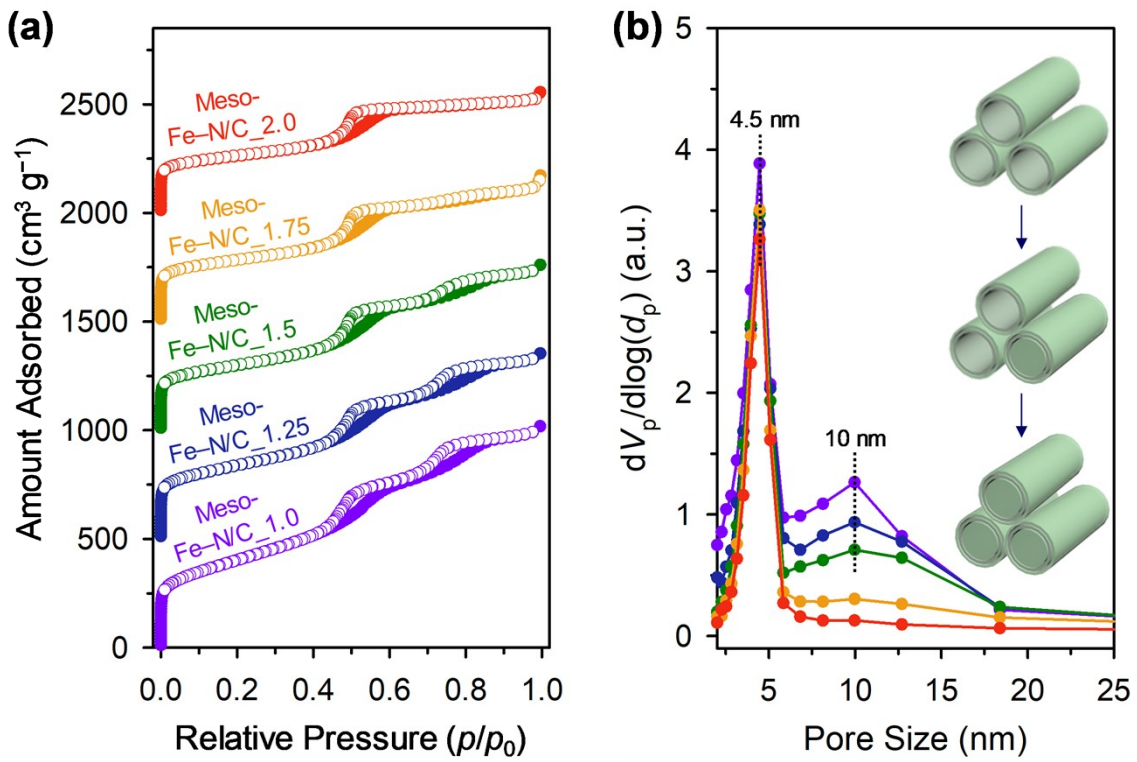


**Fig. S3** (a) N<sub>2</sub> adsorption-desorption isotherms of the Meso-Fe–N/C<sub>X</sub> catalysts. The isotherms of Meso-Fe–N/C\_1.25, Meso-Fe–N/C\_1.5, Meso-Fe–N/C\_1.75, and Meso-Fe–N/C\_2.0 are offset by 500, 1000, 1500, and 2000 cm<sup>3</sup> g<sup>-1</sup>, respectively, for clarity. (b) Pore size distribution curves obtained from the adsorption branches of the corresponding isotherms. Structural models in inset illustrate the evolution of mesopore filling with gradual increase of Fe and N precursor loading.

**Table S1.** Textural properties of the Meso-Fe–N/C\_ *X* catalysts.

Sample	BET surface area (m <sup>2</sup> g <sup>-1</sup> ) <sup>a</sup>	Pore volume (cm <sup>3</sup> g <sup>-1</sup> ) <sup>b</sup>	Pore size (nm) <sup>c</sup>
Meso-Fe–N/C_1.0	1350	1.56	4.5, 10.0
Meso-Fe–N/C_1.25	1200	1.31	4.5, 8.0–12.5
Meso-Fe–N/C_1.5	1070	1.16	4.5, 8.0–12.5
Meso-Fe–N/C_1.75	1030	1.00	4.5, 8.0–12.5
Meso-Fe–N/C_2.0	950	0.84	4.5

<sup>a</sup> Calculated in the relative pressure range of 0.05–0.3.

<sup>b</sup> Calculated at the relative pressure of 0.98–0.99.

<sup>c</sup> Calculated from the adsorption branch of the corresponding isotherm using the BJH method.

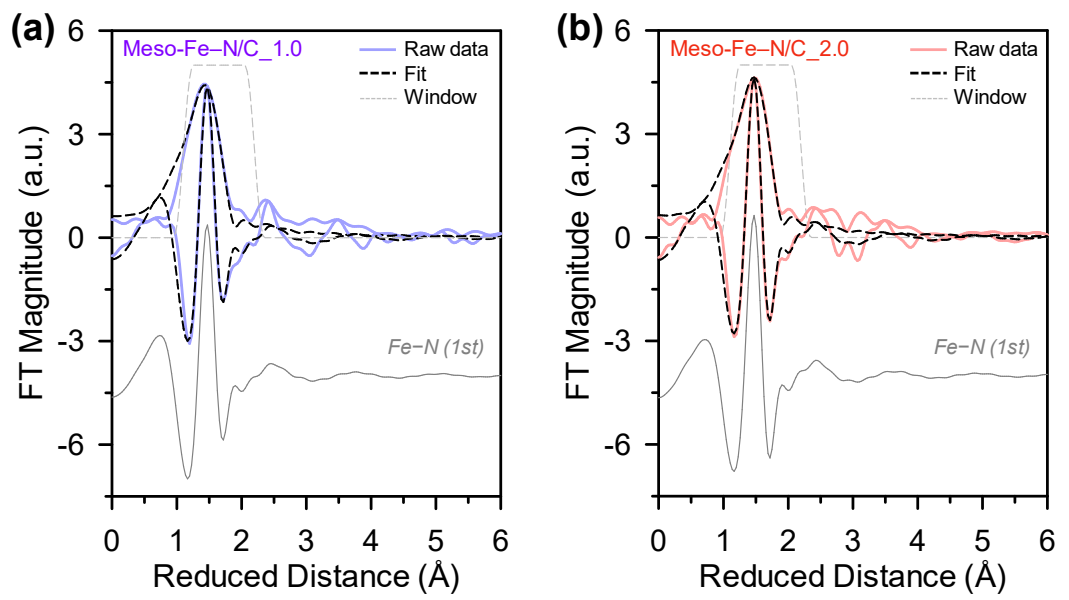


**Fig. S4** EXAFS fitting curves of (a) Meso-Fe–N/C\_1.0 and (b) Meso-Fe–N/C\_2.0 in  $R$  space.

**Table S2.** EXAFS curve fitting results of Meso-Fe–N/C\_1.0 and Meso-Fe–N/C\_2.0.

Sample	$k$ range ( $\text{\AA}^{-1}$ )	$R$ range ( $\text{\AA}$ )	Shell <sup>a</sup>	CN <sup>b</sup>	$R$ ( $\text{\AA}$ )	$\sigma^2$ ( $10^{-3} \text{\AA}^{-2}$ ) <sup>c</sup>	$\Delta E_0$ (eV)
Meso-Fe–N/C_1.0	2.5–11.5	1.1–2.2	Fe–N (1st)	5.6 ( $\pm 1.2$ )	1.96 ( $\pm 0.02$ )	13.25 ( $\pm 2.8$ )	-5.64 ( $\pm 1.20$ )
Meso-Fe–N/C_2.0	2.5–11.5	1.1–2.2	Fe–N (1st)	5.3 ( $\pm 0.6$ )	1.98 ( $\pm 0.01$ )	12.21 ( $\pm 1.59$ )	-2.42 ( $\pm 1.41$ )

<sup>a</sup>  $k^3$ -weighted fitting shell of single scattering path was noted in parentheses.

<sup>b</sup> Coordination number; the amplitude reduction factor ( $S_0^2 = 0.87$ , PAL 8C) was obtained from EXAFS fitting of Fe foil reference.

<sup>c</sup> Debye-Waller factor.

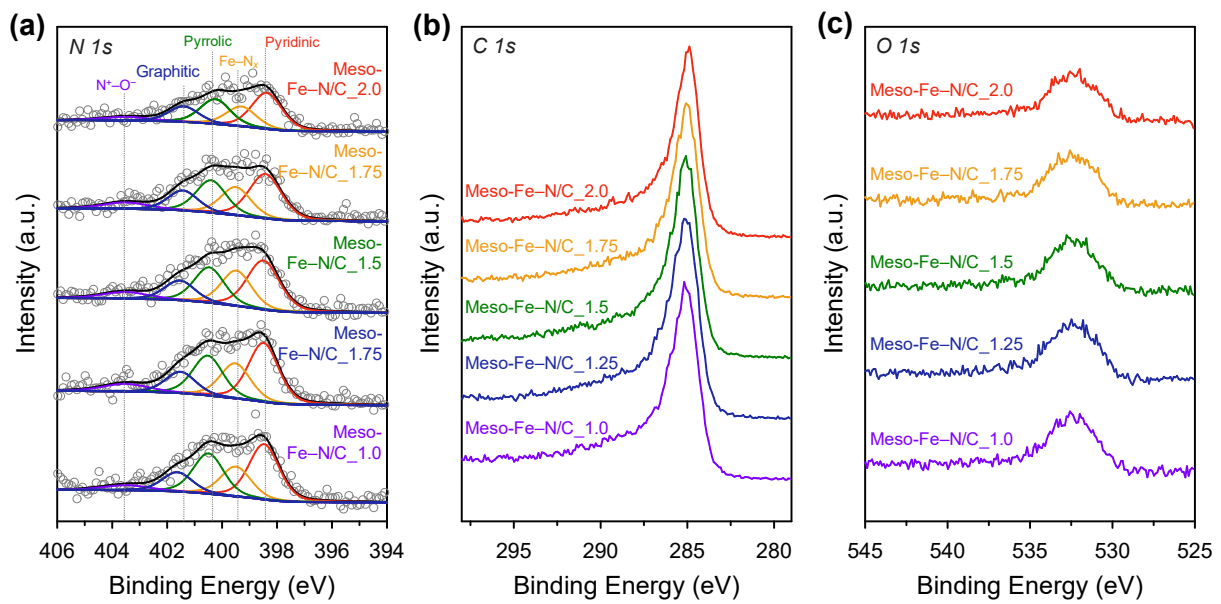


**Fig. S5** (a) Deconvoluted N 1s, (b) C 1s, and (c) O 1s XPS spectra of the Meso-Fe-N/C<sub>X</sub> catalysts.

**Table S3.** Relative peak areas for the deconvoluted N 1s XPS spectra of the Meso-Fe–N/C\_ *X* catalysts.

Sample	Relative peak area (%)				
	Pyridinic	Fe–N <sub>x</sub>	Pyrrolic	Graphitic	N <sup>+</sup> –O <sup>-</sup>
Meso-Fe–N/C_1.0	36.3	19.6	26.4	12.6	5.1
Meso-Fe–N/C_1.25	35.3	21.0	23.8	12.8	7.1
Meso-Fe–N/C_1.5	34.5	23.1	23.0	12.9	6.5
Meso-Fe–N/C_1.75	34.6	20.4	23.5	14.5	7.1
Meso-Fe–N/C_2.0	35.4	19.5	24.4	15.2	5.6

**Table S4.** Elemental analysis results of the Meso-Fe–N/C<sub>X</sub> catalysts.

Sample	Content (wt%)				
	Fe <sup>a</sup>	C <sup>b</sup>	H <sup>b</sup>	N <sup>b</sup>	O <sup>b</sup>
Meso-Fe–N/C_1.0	1.9	70.0	1.3	9.1	8.8
Meso-Fe–N/C_1.25	1.9	70.8	1.5	8.6	10.0
Meso-Fe–N/C_1.5	2.0	72.7	1.4	8.3	9.1
Meso-Fe–N/C_1.75	1.9	73.6	1.7	8.0	9.2
Meso-Fe–N/C_2.0	2.0	73.9	1.6	7.2	7.9

<sup>a</sup> Obtained by an inductively coupled plasma optical emission spectrometer.

<sup>b</sup> Obtained by a combustion element analyzer.

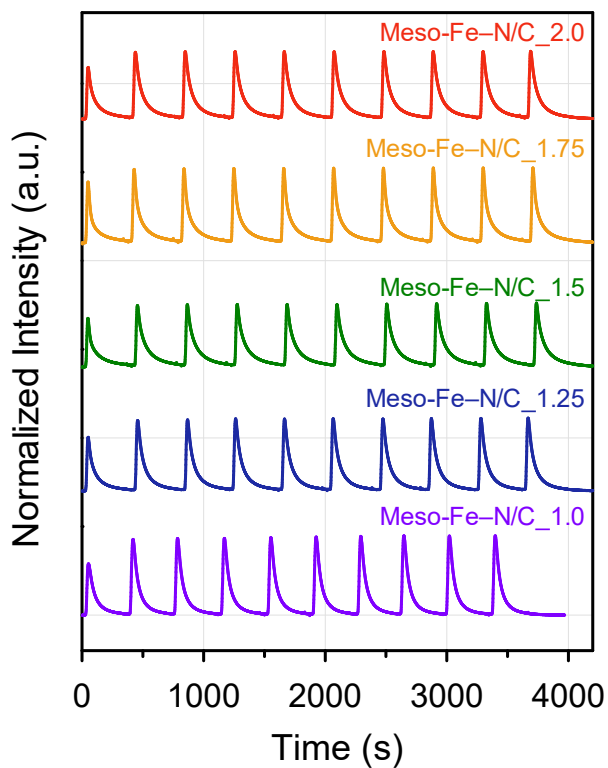


**Fig. S6** CO pulse cryo-adsorption profiles of the  $\text{Meso-Fe-N/C}_X$  catalysts measured at  $-80^\circ\text{C}$ .

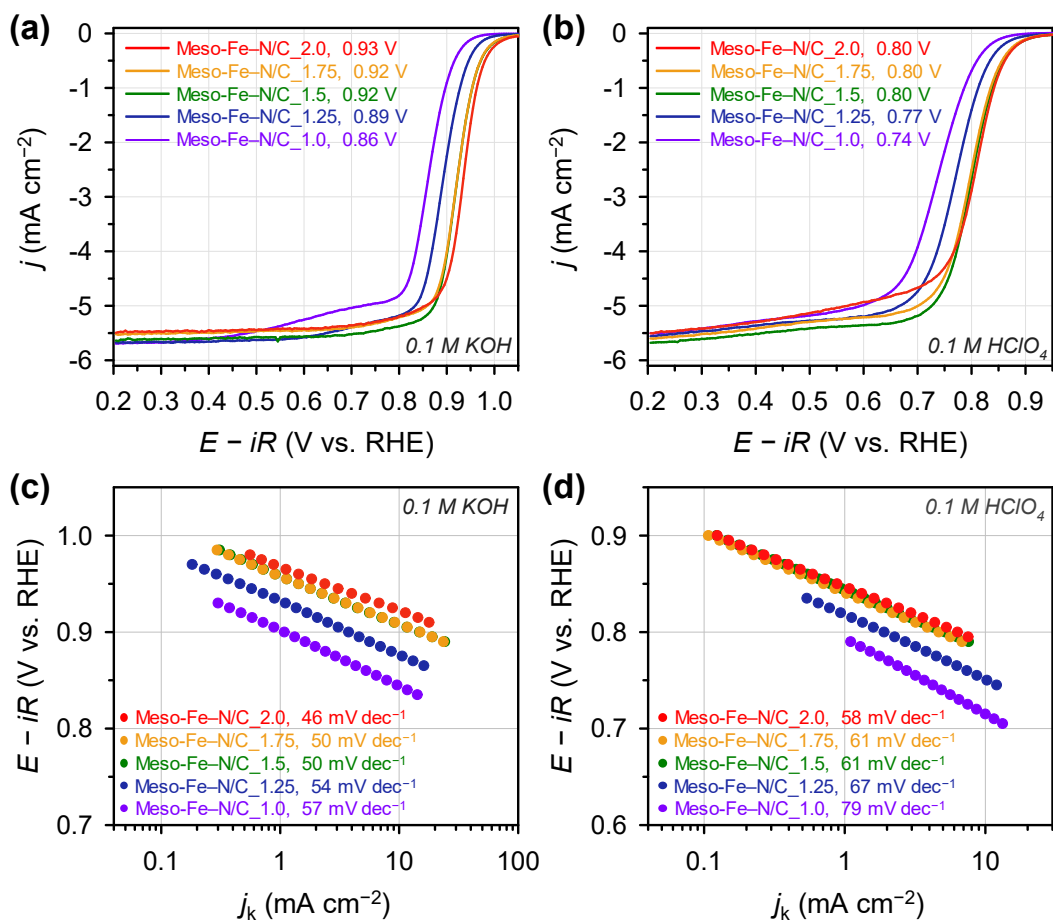


**Fig. S7** ORR polarization curves of the Meso-Fe–N/C<sub>\_X</sub> catalysts in (a) 0.1 M KOH and (b) 0.1 M HClO<sub>4</sub> electrolytes. Tafel slopes of the Meso-Fe–N/C<sub>\_X</sub> catalysts in (c) 0.1 M KOH and (d) 0.1 M HClO<sub>4</sub> electrolytes.

**Table S5.** Site density and ORR activity parameters of the Meso-Fe–N/C\_ *X* catalysts in 0.1 M KOH.

Sample	Site density (sites g <sup>-1</sup> ) <sup>a</sup>	<i>j</i> <sub>k</sub> (mA cm <sup>-2</sup> ) <sup>b</sup>	<i>MA</i> (mA mg <sup>-1</sup> ) <sup>c</sup>	TOF (e <sup>-</sup> site <sup>-1</sup> s <sup>-1</sup> ) <sup>d</sup>
Meso-Fe–N/C_1.0	$4.7 \times 10^{19}$	1.1	1.83	0.25
Meso-Fe–N/C_1.25	$3.5 \times 10^{19}$	3.8	6.33	1.12
Meso-Fe–N/C_1.5	$4.5 \times 10^{19}$	14.8	24.7	3.44
Meso-Fe–N/C_1.75	$3.7 \times 10^{19}$	15.0	25.0	4.23
Meso-Fe–N/C_2.0	$3.5 \times 10^{19}$	25.9	43.2	7.77

<sup>a</sup> Derived from CO cryo chemisorption.

<sup>b</sup> Kinetic current density calculated at 0.9 V.

<sup>c</sup> Mass activity calculated at 0.9 V.

<sup>d</sup> Turnover frequency calculated at 0.9 V.

**Table S6.** Benchmarking TOF of Meso-Fe–N/C\_2.0 in alkaline media with those of previously reported Fe–N/C catalysts.

Sample	Site density (sites g <sup>-1</sup> ) <sup>a</sup>	TOF (e <sup>-</sup> site <sup>-1</sup> s <sup>-1</sup> ) <sup>b</sup>	Ref
<b>Meso-Fe–N/C_2.0</b>	<b><math>3.5 \times 10^{19}</math></b>	<b>7.77</b>	<b>This work</b>
Fe <sub>0.5</sub> NC-800	$3.99 \times 10^{19}$	0.46	1
ZIF-Fe	$4.39 \times 10^{19}$	1.21	2

<sup>a</sup> Determined by CO cryo-chemisorption.

<sup>b</sup> Turnover frequency calculated at 0.9 V.

**Table S7.** Site density and ORR activity parameters of the Meso-Fe–N/C\_X catalysts in 0.1 M HClO<sub>4</sub>.

Sample	Site density (sites g <sup>-1</sup> ) <sup>a</sup>	$j_k$ (mA cm <sup>-2</sup> ) <sup>b</sup>	MA (mA mg <sup>-1</sup> ) <sup>c</sup>	TOF (e <sup>-</sup> site <sup>-1</sup> s <sup>-1</sup> ) <sup>d</sup>
Meso-Fe–N/C_1.0	$4.7 \times 10^{19}$	0.8	1.33	0.18
Meso-Fe–N/C_1.25	$3.5 \times 10^{19}$	1.9	3.17	0.56
Meso-Fe–N/C_1.5	$4.5 \times 10^{19}$	5.2	8.67	1.21
Meso-Fe–N/C_1.75	$3.7 \times 10^{19}$	4.7	7.83	1.32
Meso-Fe–N/C_2.0	$3.5 \times 10^{19}$	6.3	10.5	1.89

<sup>a</sup> Active surface site density derived from CO chemisorption.

<sup>b</sup> Kinetic current density calculated at 0.9 V.

<sup>c</sup> Mass activity calculated at 0.9 V.

<sup>d</sup> Turnover frequency calculated at 0.8 V.

**Table S8.** Benchmarking TOF of Meso-Fe–N/C\_2.0 in acidic media with those of previously reported Fe–N/C catalysts.

Sample	Site density (sites g <sup>-1</sup> ) <sup>a</sup>	TOF (e <sup>-</sup> site <sup>-1</sup> s <sup>-1</sup> ) <sup>b</sup>	Ref
<b>Meso-Fe–N/C_2.0</b>	<b><math>3.5 \times 10^{19}</math></b>	<b>1.89</b>	<b>This work</b>
Fe <sub>0.5</sub> NC-800	$3.99 \times 10^{19}$	0.45	1
ZIF-Fe	$4.39 \times 10^{19}$	0.49	2
FeMn~RP	$6.7 \times 10^{19}$	1.6	3,5
FeRP c	$0.72 \times 10^{19}$	1.55	4,5
PANI-CM	$3.79 \times 10^{19}$	1.18	6,7
FeNC	$9.76 \times 10^{19}$	0.156	8
PAJ	$2.02 \times 10^{19}$	0.71	9

<sup>a</sup> Derived from CO cryo-chemisorption.

<sup>b</sup> Turnover frequency calculated at 0.8 V.

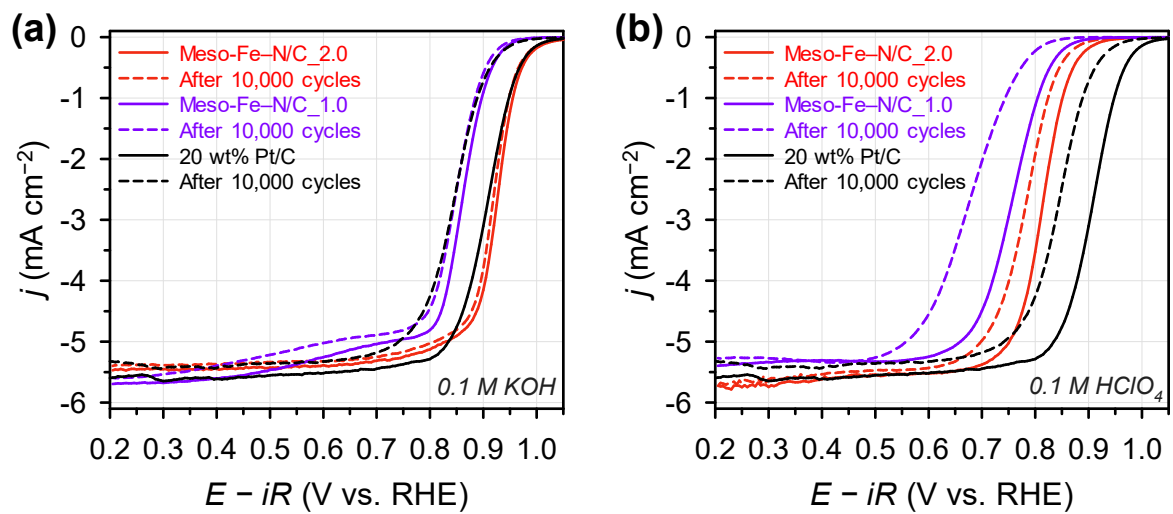


**Fig. S8** ORR polarization curves for the ORR activity of the Meso-Fe-N/C\_1.0, Meso-Fe-N/C\_2.0, and Pt/C before and after 10,000 potential cycles in a)  $0.1 \text{ M KOH}$  and b)  $0.1 \text{ M HClO}_4$ .

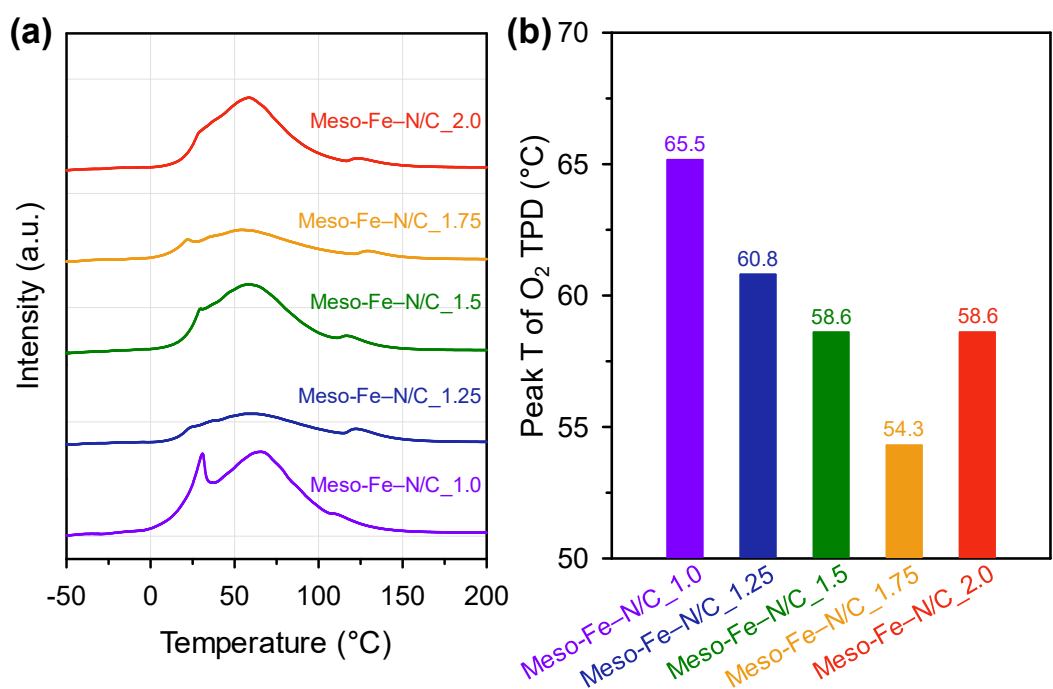


**Fig. S9** (a) O<sub>2</sub> TPD profiles and (b) second O<sub>2</sub> desorption peak temperatures of the Meso-Fe–N/C<sub>X</sub> catalysts.

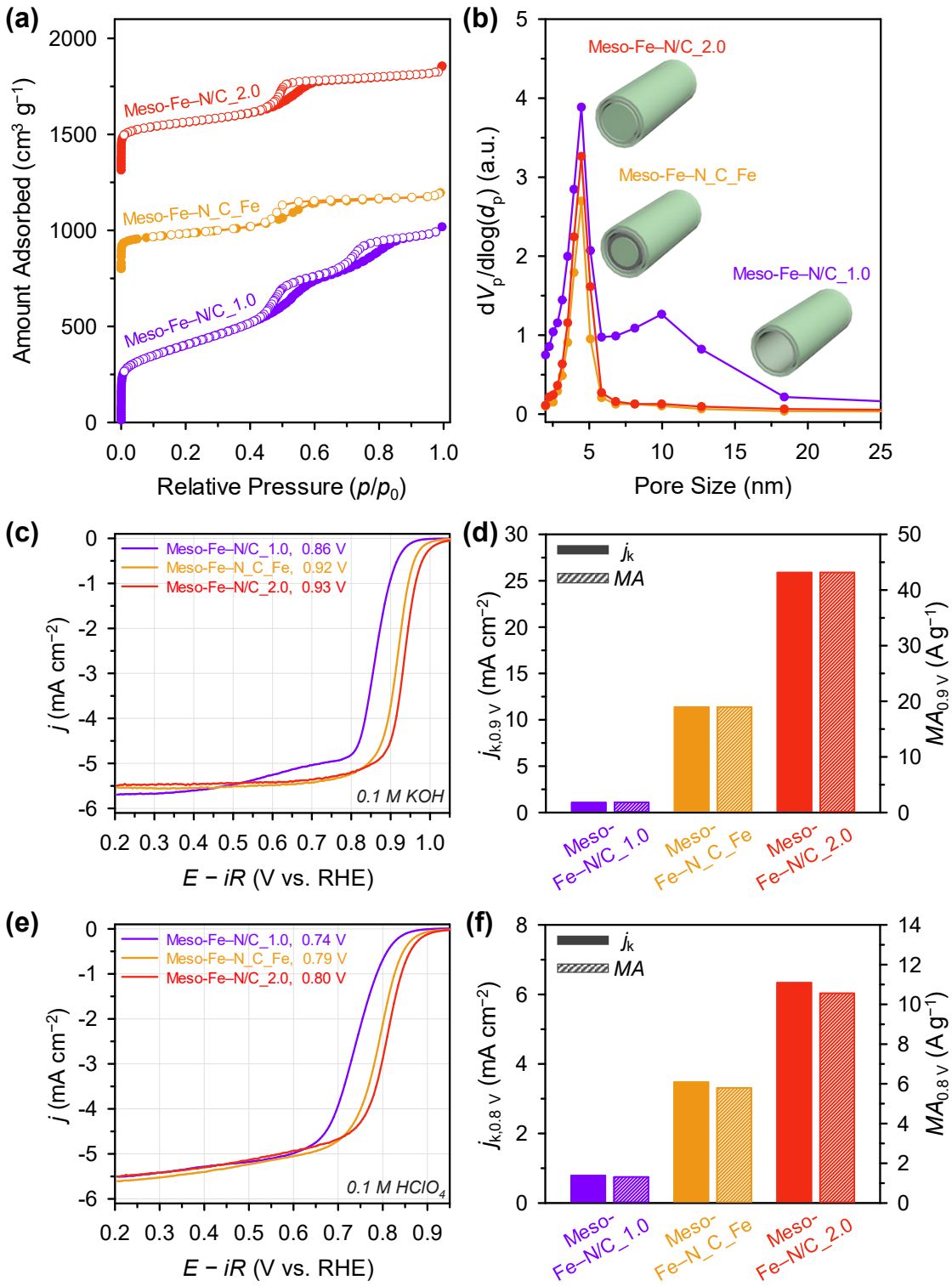


**Fig. S10** (a) N<sub>2</sub> adsorption-desorption isotherms of Meso-Fe-N/C\_1.0, Meso-Fe-N/C\_Fe, and Meso-Fe-N/C\_2.0. The isotherms of Meso-Fe-N/C\_Fe and Meso-Fe-N/C\_2.0 are offset by 800 and 1300 cm<sup>3</sup> g<sup>-1</sup>, for clarity. (b) Pore size distribution curves obtained from the adsorption branches of the corresponding isotherms with structural models for respective catalyst. (c and e) ORR polarization curves of Meso-Fe-N/C\_1.0, Meso-Fe-N/C\_Fe, and Meso-Fe-N/C\_2.0 in (c) 0.1 M KOH and (e) 0.1 M HClO<sub>4</sub> electrolytes. (d and f) Bar graphs comparing ORR kinetic current density and mass activity in (d) 0.1 M KOH and (f) 0.1 M HClO<sub>4</sub> electrolytes.

### 3. References

- 1 F. Luo, C. H. Choi, M. J. M. Primbs, W. Ju, S. Li, N. D. Leonard, A. Thomas, F. Jaouen and P. Strasser, *ACS Catal.*, 2019, **9**, 4841–4852.
- 2 F. Luo, S. Wagner, W. Ju, M. Primbs, S. Li, H. Wang, U. I. Kramm and P. Strasser, *J. Am. Chem. Soc.*, 2022, **144**, 13487–13498.
- 3 N. R. Sahraie, U. I. Kramm, J. Steinberg, Y. Zhang, A. Thomas, T. Reier, J.-P. Paraknowitsch and P. Strasser, *Nat. Commun.*, 2015, **6**, 8618.
- 4 M. Primbs, Y. Sun, A. Roy, D. Malko, A. Mehmood, M.-T. Sougrati, P.-Y. Blanchard, G. Granozzi, T. Kosmala, G. Daniel, P. Atanassov, J. Sharman, C. Durante, A. Kucernak, D. Jones, F. Jaouen and P. Strasser, *Energy Environ. Sci.*, 2020, **13**, 2480–2500.
- 5 S. Specchia, P. Atanassov and J. H. Zagal, *Curr. Opin. Electrochem.*, 2021, **27**, 100687.
- 6 H. T. Chung, D. A. Cullen, D. Higgins, B. T. Snead, E. F. Holby, K. L. More and P. Zelenay, *Science*, 2017, **357**, 479–484.
- 7 N. D. Leonard, S. Wagner, F. Luo, J. Steinberg, W. Ju, N. Weidler, H. Wang, U. I. Kramm and P. Strasser, *ACS Catal.*, 2018, **8**, 1640–1647.
- 8 F. Luo, A. Roy, L. Silvioli, D. A. Cullen, A. Zitolo, M. T. Sougrati, I. C. Oguz, T. Mineva, D. Teschner, S. Wagner, J. Wen, F. Dionigi, U. I. Kramm, J. Rossmeisl, F. Jaouen and P. Strasser, *Nat. Mater.*, 2020, **19**, 1215–1223.
- 9 M. Primbs, Y. Sun, A. Roy, D. Malko, A. Mehmood, M.-T. Sougrati, P.-Y. Blanchard, G. Granozzi, T. Kosmala, G. Daniel, P. Atanassov, J. Sharman, C. Durante, A. Kucernak, D. Jones, F. Jaouen and P. Strasser, *Energy Environ. Sci.*, 2020, **13**, 2480–2500.